Geosystems and Geoenvironment 2 (2023) 100193

Contents lists available at ScienceDirect

Geosystems and Geoenvironment

journal homepage: www.elsevier.com/locate/geogeo

Numerical modeling of small-scale unsaturated soil slope subjected to transient rainfall

Chang Liu[a,*], Yipu Yan[b], Hao-Qing Yang[c]

[a] College of Liberal Arts and Sciences, Iowa State University of Science and Technology, IA 50011, United States of America
[b] School of Architecture Engineering, Jinling Institute of Technology, Nanjing 211169, China
[c] School of Civil and Environmental Engineering, Nanyang Technological University, 639798, Singapore

ARTICLE INFO

Article history:
Received 25 November 2022
Revised 1 February 2023
Accepted 29 March 2023

Handling Editor: Zhong-Hai Li

Keywords:
Slope
Rainfall
Unsaturated soil
Matric suction
Richards' equation
Extended Barcelona basic model

ABSTRACT

Climate change is creating more extreme rain events and causing more landslides in recent years. Most of the previous studies focused on large-scale slopes such as mountainous areas. For the problem of small-scale landslides in urban areas, a hydro-mechanical analysis of soil slopes under rainfall is also demanded. In this study, a numerical model of a slope under rainfall and load is established by COMSOL Multiphysics. To facilitate the analysis for practical purposes, two built-in modules are used to model a unidirectional coupling of hydro-mechanical behaviors of unsaturated soil slopes. The Richards' module is first adopted to model an unsaturated soil slope under rainfall. Then the Extended Barcelona Basic module that considers the matric suction is adopted as the constitutive model. The effect of rainfall duration and saturated hydraulic conductivity on stress, settlement, and pore-water pressure are studied. When the rainfall proceeds, the matric suction head keeps reducing constantly. For a fixed location, the settlement decreases as k_s increases. The wetting front is more apparent as the k_s is reduced as the curvature of the pore pressure profile is more pronounced. The matric suction at a steady state is decreased when the k_s becomes small. The simulated soil suction is comparable to these field monitoring data.

1. Introduction

Rainfall is one of the most common drivers for landslides. Climate change is creating more extreme rain events and causing more landslides in recent years (Yang et al., 2022). Therefore, it is of great significance to study the behaviors of slopes under rainfall.

Infiltration plays a significant role in the instability of slopes under rainfall conditions (Zhang et al., 2004; Yang et al., 2020; Li et al., 2023). Pore-water pressure changes due to rainfall infiltration and seepage will lead to changes in stresses and deformation (Yang et al., 2021; Wei et al., 2021; Deng et al., 2022; Zhang et al., 2022). The hydro-mechanical behaviors of the slopes under rainfall have been studied by many researchers. Zhang et al. (2005) developed a coupled hydro-mechanical model to study the behavior and stability of deformable unsaturated soil slopes in a probabilistic study. Borja et al. (2012) presented a methodology for quantifying deformation, stresses, saturation, fluid flow, and factor of safety for a steep hillside slope subjected to rainfall infiltration. Qi and Vanapalli (2015) evaluated the coupling effect or swelling on the hydraulic response as well as the stability of the surficial layer of a typical expansive soil slope. Yang et al. (2017) presented a case study and numerical investigation of two unstable unsaturated slopes along the Taipei Maokong Gondola system. Yeh and Tsai (2018) studied a coupled hydro-mechanical framework based on transient seepage analysis and slope stability analysis to investigate the effects of hydraulic conductivity anisotropy on rainfall infiltration and slope safety at various slope locations. Ni et al. (2018) developed a model that can quantify the mechanical and hydrological effects and their relative contribution to the stability of an unsaturated vegetated coarse-grained soil slope. Zhang et al. (2018) presented a probabilistic calibration method for coupled hydro-mechanical modeling of slope stability with the integration of multiple types of measurements. These studies illustrated that a coupled hydro-mechanical analysis is preferred to analyze the behavior and stability of a slope subjected to rainfall.

Nevertheless, most of the previous studies focused on large-scale slopes such as mountainous areas. For the problem of small-scale landslides in urban areas, a hydro-mechanical analysis of soil slopes under rainfall is also demanded. Small-scale landslides have consistently been a topic in the interest of model tests due to the

* Corresponding author.
E-mail address: changliu970618@gmail.com (C. Liu).

https://doi.org/10.1016/j.geogeo.2023.100193

huge budget and time of the field prototype test (Liang et al., 2017; Olivares, 2007). The numerical simulation of the small-scale landslides is always used to compare to the model test. More importantly, geological engineers noticed that small-scale landslides result in more severe consequences than those due to very large ones (Yang et al., 2023; Crosta et al., 2005). The small-scale landslides have been studied extensively recently, especially in the submarine and urban area (Kelner et al., 2016; Casalbore et al., 2020; Cui et al., 2020). In terms of rainfall-induced landslides, it is discovered that the hydro-mechanical responses of small-scale slopes are different from the large ones. Rahardjo et al. (1998) concluded that large landslides occurred after a 24 h rainfall of over 110 mm and that small landslides occurred after significant amounts of antecedent rainfall. Wang et al. (2021) revealed that the suction strength is a dominant component of shear strength in maintaining stable conditions in small-scale loess slopes, but large-scale landslides are mainly controlled by the frictional strength of the slider. Pajalić et al. (2021) found that small-scale slopes lead to relatively low confining pressure and the strength associated with soil suction may be dominant compared to the total shear strength and thus play a major role in keeping the slope stability under rainfall. It can be concluded he soil suction is more dominant in small slopes, due to the fact that rainfall-induced slope failures are normally shallow with a depth of less than 3 m (Zhang et al., 2011, 2014). Therefore, hydro-mechanical analysis with an emphasis on soil suction of small slopes may be of benefit to rainfall-induced landslides.

In Singapore, small-scale landslides (generally smaller than 10 m in height) have frequently occurred due to the frequent rainfall (Pitts et al., 1984; Toll, 2001; Satyanaga et al., 2021). Since Singapore is a highly urbanized and densely populated country, small-scale landslides may also lead to severe consequences. On September 2nd, 2022, a small-scale landslide occurred at a construction site in Clementi in the event of heavy rainfall (Fig. 1) caused a passerby injured and damage to a road. Much attention should be paid to these small-scale landslides in Singapore. Preliminary hydro-mechanical analysis promptly for further disaster mitigation is in demand. A timely and reliable hydro-mechanical analysis of unsaturated soil slopes is necessary for practical purposes.

In this study, a numerical model of a slope under rainfall and load is established by COMSOL Multiphysics. To facilitate the analysis for practical purposes, two built-in modules are used to model a unidirectional coupling of hydro-mechanical behaviors of unsaturated soil slopes. The Richards' module is first adopted to model an unsaturated soil slope under rainfall. Then the Extended Barcelona Basic module that considers the matric suction is adopted as the constitutive model. The effect of rainfall duration and saturated hydraulic conductivity on stress, settlement, and pore-water pressure are studied.

2. Numerical model of unsaturated soil slope under rainfall

2.1. Hydraulic behavior

Richard's equation is used to represent the movement of water in unsaturated soils (Richard, 1931; Farthing and Ogden, 2017):

$$\frac{\partial \theta(h)}{\partial t} = \nabla \cdot k(h) \nabla H \tag{1}$$

where h is pore pressure head; t is time; H is the hydraulic head; $k(h)$ denotes unsaturated hydraulic conductivity depending on soil suction h (i.e., negative pressure head) and $\theta(h)$ is the volumetric water content related to h.

In this study, the exponential soil-water characteristic curve (SWCC) is adopted and can be expressed as (Sillers and Fredlund, 2001)

$$S_e = \frac{\theta(h) - \theta_r}{\theta_s - \theta_r} = \begin{cases} \exp(-\alpha h) h < 0 \\ 1 \quad h > 0 \end{cases} \tag{2}$$

where S_e is the normalized volumetric water content; θ_s and θ_r are the saturated volumetric water content and residual volumetric water content, respectively; α is the fitting parameter.

The permeability function is based on Leong and Rahardjo (1997):

$$k(h) = K_s S_e^{\beta} \tag{3}$$

where K_s is the saturated coefficient of permeability and β is the fitting parameter.

Fig. 1. Landslide on 2 September 2022 at the Clementi construction site, Singapore.

2.2. Elastoplastic behavior model of unsaturated soils

The extended Barcelona Basic model (BBMx) (Pedroso and Farias, 2011) is an extension of the modified Cam-Clay model (Wood, 1990; Tamagnini, 2004). It is extended to simulate the plastic behaviors of unsaturated soils with the concept of the critical state model (Alonso et al., 1990). The soil suction is considered as an extra state variable in BBMx. It not only affects the water flow in unsaturated soils, but also influences the mechanical response of soils.

2.2.1. Elastic response

In the BBMx model, the total volumetric elastic strain $\varepsilon_{e,vol}$ is a combination of elastic strains by pressure and suction:

$$\varepsilon_{e,vol} = \varepsilon^{\sigma}_{e,vol} + \varepsilon^{s}_{e,vol} \tag{4}$$

where $\varepsilon^{\sigma}_{e,vol}$ and $\varepsilon^{s}_{e,vol}$ are the elastic strains by pressure and suction, respectively.

The volumetric elastic strain by pressure is calculated as

$$\boldsymbol{\varepsilon}^{\sigma}_{e,vol} = -\frac{dp}{K} \tag{5}$$

where K is the bulk modulus and p is the mean stress.

The volumetric elastic response due to suction is given by

$$\varepsilon^{s}_{e,vol} = -\frac{\kappa_s}{1+e_0}\ln\left(\frac{s+p_{atm}}{s_0+p_{atm}}\right) \tag{6}$$

where $s=|h|$ and is suction and s_0 is the initial suction; κ_s is the swelling index for changes in suction; p_{atm} is the atmospheric pressure and e_0 is the initial void ratio.

The stress tensor $\boldsymbol{\sigma}$ is written as

$$\boldsymbol{\sigma} = \mathrm{dev}(\boldsymbol{\sigma}_0) + p\mathbf{I} + 2G\mathrm{dev}(\boldsymbol{\varepsilon}_e) \tag{7}$$

where $\mathbf{I}$ is the identity matrix; $\boldsymbol{\varepsilon}_e$ is the elastic strain tensor; $\boldsymbol{\sigma}_0$ is the initial or external stress tensor; G is the shear modulus and dev denotes the deviator operator.

2.2.2. Plastic response

The plastic strain rate $\dot{\varepsilon}_p$reads:

$$\dot{\varepsilon}_p = \lambda_p\left(-\frac{1}{3}\frac{\partial Q_p}{\partial p}\mathbf{I} + \frac{\partial Q_p}{\partial q}\frac{3}{2q}\mathrm{dev}(\boldsymbol{\sigma})\right) \tag{8}$$

where Q_p is a plastic potential; q is the deviator stress and λ_p is the plastic multiplier.

According to the associated flow rule, a plastic potential Q_p is the same as yield function F_y:

$$Q_p = F_y \tag{9}$$

The yield function F_y of BBM is defined as

$$F_y = q^2 + M^2(p-p_{cs})(p+p_s) + p^2_{ref}\left(\exp\left(\frac{b(s-s_y)}{p_{ref}}\right) - \exp\left(\frac{-bs_y}{p_{ref}}\right)\right) \tag{10}$$

where p and q are stress invariants; p_{cs} is the consolidation pressure at current suction, p_s is the tensile strength due to current suction; b is a dimensionless smoothing parameter; s_y is the yield value at current suction, and p_{ref} is the reference pressure at which the reference void ratio e_{ref} was measured.

The slope of the critical state line M is expressed as:

$$M = \frac{6\sin\phi}{3-\sin\phi} \tag{11}$$

where ϕ is the friction angle of a soil.

The consolidation pressure at the current suction p_{cs} is calculated from

$$p_{cs} = p_{ref}\left(\frac{p_c}{p_{ref}}\right)^{\left(\frac{\lambda_0-\kappa}{\lambda(s)-\kappa}\right)} \tag{12}$$

where $\lambda(s)$ is the compression index at current suction, λ_0 is the compression index at saturation, and κ is the swelling index. The compression index at current suction, $\lambda(s)$, is given by

$$\lambda(s) = \lambda_0((1-w)e^{-\frac{s}{m}} + w) \tag{13}$$

where w and m are weighting and soil stiffness parameters.

The hardening is controlled by the evolution of the consolidation pressure p_c, which depends on the volumetric plastic strain $\boldsymbol{\varepsilon}_{p,vol}$:

$$\dot{p}_c = -\frac{1+e_0}{\lambda_0-\kappa}p_c\dot{\varepsilon}_{p,vol} \tag{14}$$

The evolution of the yield value at the current suction s_y is also governed by $\boldsymbol{\varepsilon}_{p,vol}$ as

$$\dot{s}_y = -\frac{1+e_0}{\lambda_s-\kappa_s}(s_y+p_{atm})\dot{\varepsilon}_{p,vol} \tag{15}$$

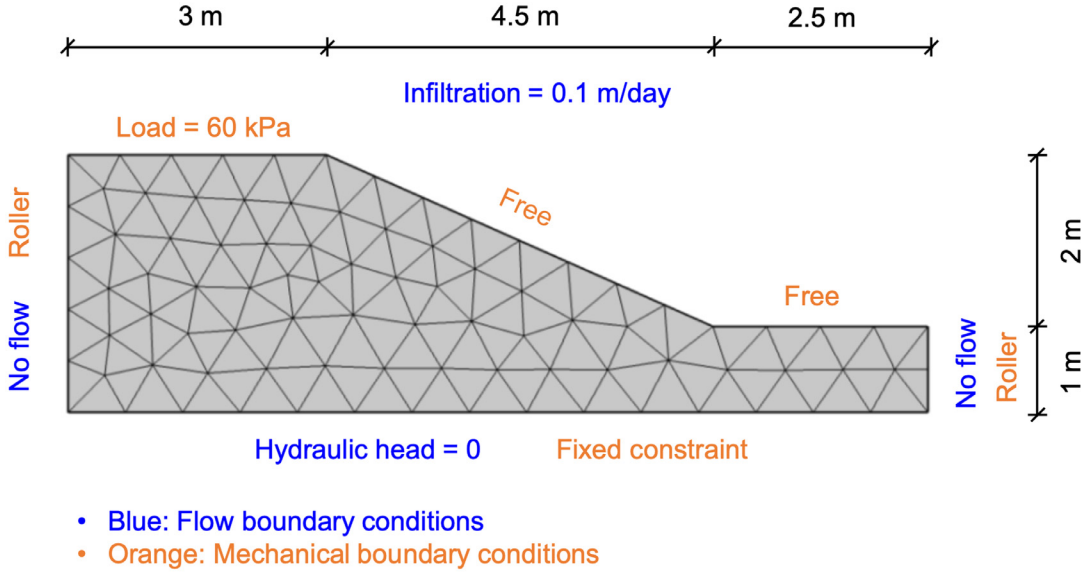

Fig. 2. Geometry, mesh, and boundary conditions of slope model.

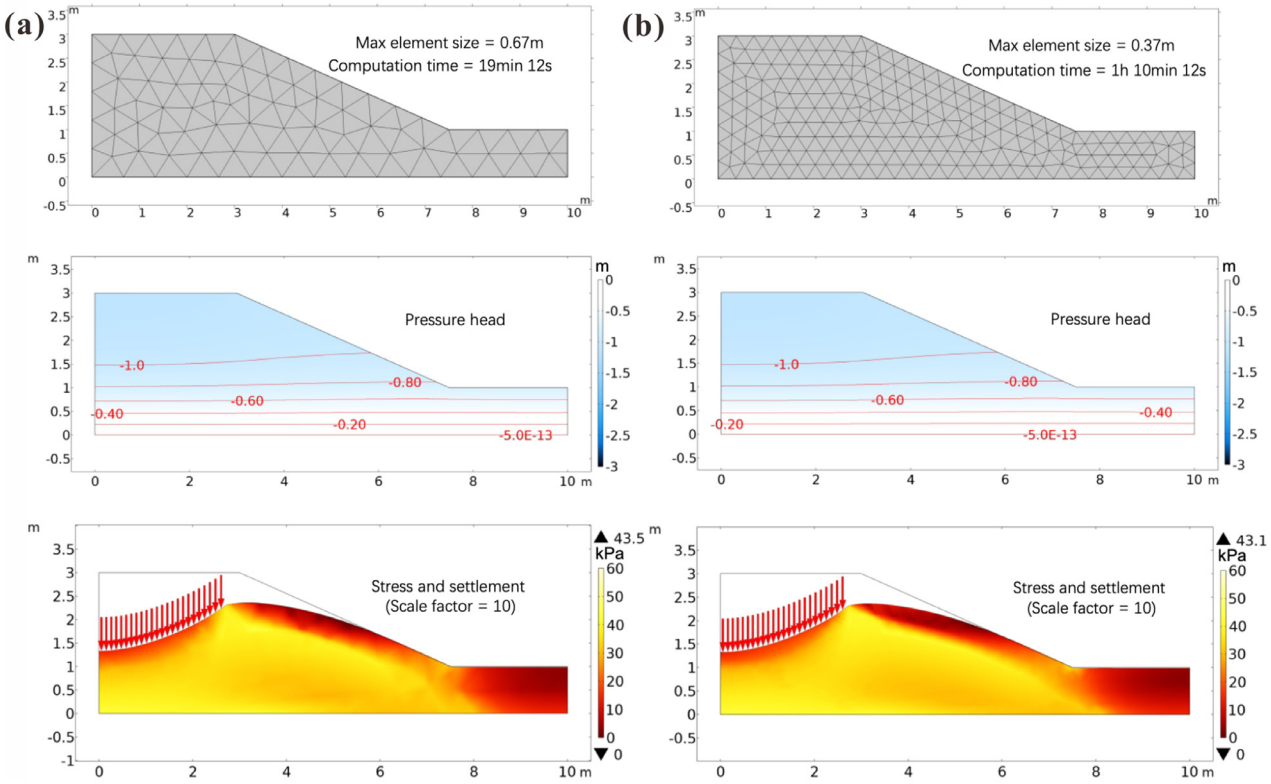

Fig. 3. Effect of mesh grid on numerical results ($t = 1$ d): (a) Coarse mesh, (b) Fine mesh.

where λ_s is the compression index for changes in suction.

It is widely accepted that rainfall-induced landslides are the rapid movements of soils due to the sudden changes in pore water pressure and seepage force. Therefore, the viscosity of unsaturated soils is enough large and can be omitted. The viscoplastic straining (i.e., creep) is not regularly considered for the modeling rainfall-induced slope failures. Based on the viscoplastic concept given by Perzyna (1966), the BBMx can be extended to a viscoplastic model. The viscoplastic strain is calculated by multiplying a viscosity parameter in the flow function. For more details, one can refer to Thanh et al. (2019).

The Richards' equation and the BBMx model are both built-in modules of COMSOL Multiphysics. The hydro-mechanical model is not fully coupling where changes in pore pressure affect the soil deformation, but changes in the deformation have no effect on the pore pressure.

2.3. Modeling of unsaturated soil slope

The numerical model of unsaturated soil slope under rainfall is simulated by COMSOL Multiphysics. Richard's equation and BBMx are the built-in modules. The soil type is assumed to be clay. The hydraulic parameters are based on the data from Abed and Vermeer (2009). The parameters of BBM are set as default by Navarro et al. (2014). The model parameters are summarized in Table 1.

Fig. 2 shows the geometry, mesh, and boundary conditions of the slope model. The height of the slope is 3 m and the width is 9 m. The slope ratio is 2:4.5. It assumes that the slope is supported by a rigid base and a fixed constraint is applied on the lower boundary. The groundwater table is assumed at the lower boundary and the hydraulic head is set to be 0 m. A roller boundary is used on both the left and right boundaries with no flow passing through them. A load of 60 kPa is applied on the slope crest to represent road weight. No constraints and no load are acting on the other top boundaries, which is denoted as free in COMSOL. The infiltration rate is set to be 0.1 m/day on the top as the hydraulic boundary condition.

Table 1
Parameters for the hypothetical slope.

Parameters	Definition	Value	Unit
ν	Poisson's ratio	0.2	
ρ_s	Soil density	1743	kg/m^3
ρ_w	Water density	1000	kg/m^3
μ_w	Dynamic viscosity of water	0.001	Pa·s
κ	Swelling index	0.006	
κ_s	Swelling index for changes in suction	0.008	
λ	Compression index at saturation	0.22	
λ_s	Compression index for changes in suction	0.123	
M	Slope of critical state line	1.24	
w	Weight parameter	0.4	
m	Soil stiffness parameter	60	kPa
b_s	Plastic potential smoothing parameter	10	
k_b	Tension to suction ratio	0.6	
s_y	Initial yield value for suction	100	kPa
e_0	Initial void ratio	0.666	
p_{ref}	Reference pressure	10	kPa
p_{c0}	Initial consolidation pressure	50	kPa
Φ	Initial porosity	0.4	
k_s	Saturated hydraulic conductivity	1	m/day
α	Fitting parameter of SWCC	2	1/m
p	Fitting parameter of SWCC	0	
θ_{res}	Residual degree of saturation	0.1	
θ_{sat}	Degree of saturation at full saturation	0.4	

The results of pressure head, stress, and settlement based on different mesh grid is shown in Fig. 3. A coarse mesh is used in Fig. 3a with a maximum size of 0.67 m. By contrast, a fine mesh with a maximum size of 0.37 m is used in Fig. 3b. The results of the two mesh grids are almost the same. Only the maximum stress of coarse mesh (43.5 kPa) is slightly larger than it in fine mesh (43.1 kPa). However, the computational time rises from

around 19 min to more than 70 min. It illustrates that the coarse mesh used in Fig. 2 is a cost-effective choice.

3. Results and discussions

Fig. 4 shows the variation in the degree of saturation of the soil slope. Fig. 4a shows the initial condition of the soil slope. The degree of saturation is 1 at the bottom of the slope where the water table lies. The degree of saturation decreases towards the top of the slope and it ends up below 0.1. Fig. 4b, c, and d shows the degree of saturation after rainfall started at $t = 0.1$ d, $t = 0.2$ d, and $t = 0.3$ d, respectively. The contour for saturation of 0.1 rises towards the surface as time goes on. It indicates that the unsaturated soil slope becomes more saturated as rainfall happens.

Fig. 5 is the variation of pressure head in the soil slope after rainfall. Fig. 5a shows the initial pressure head of the slope. The

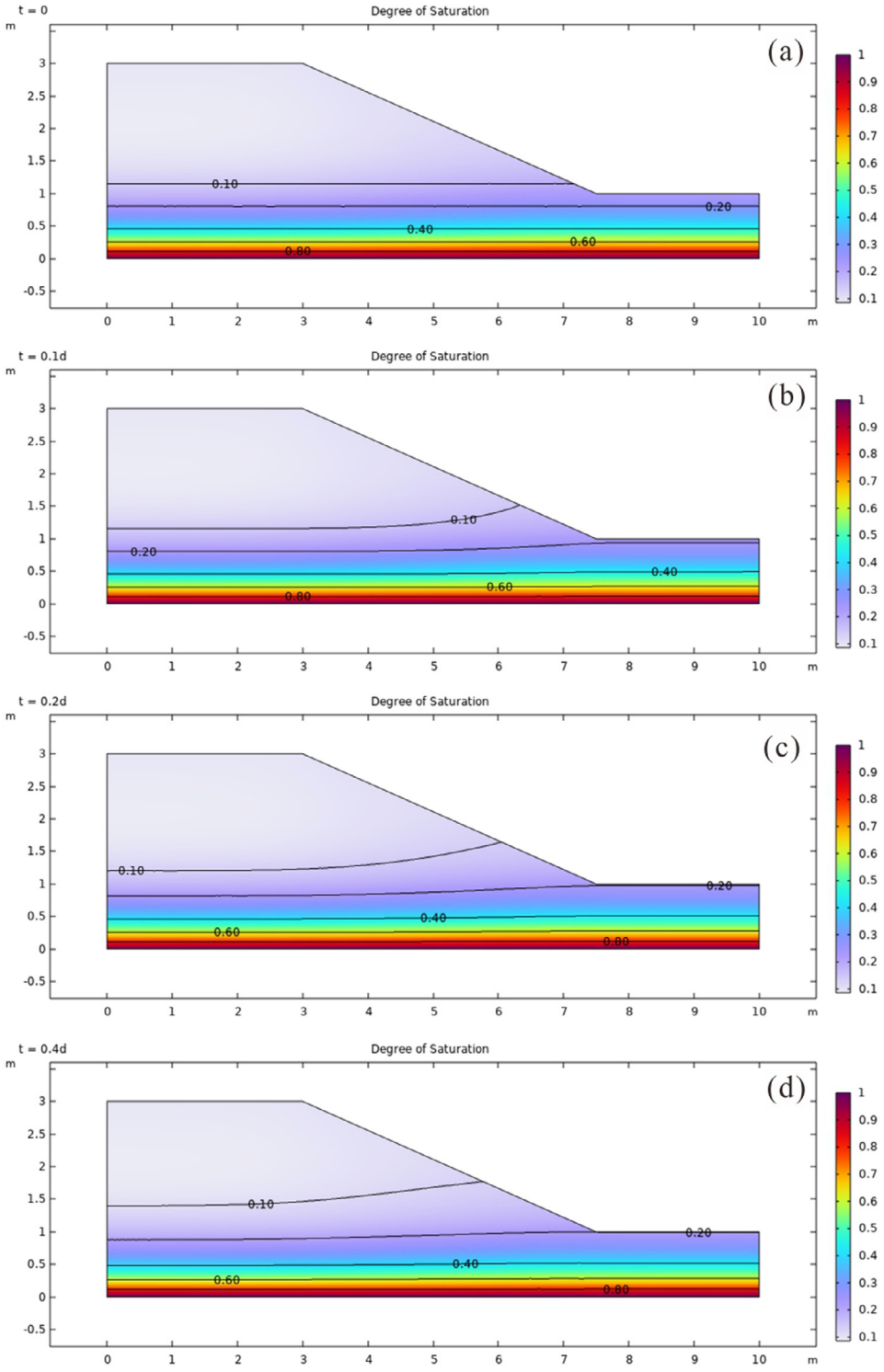

Fig. 4. Variation of degree of saturation after rainfall: (a) $t = 0$; (b) $t = 0.1$ *d*; (c) $t = 0.2$ *d*; (d) $t = 0.4$ *d*

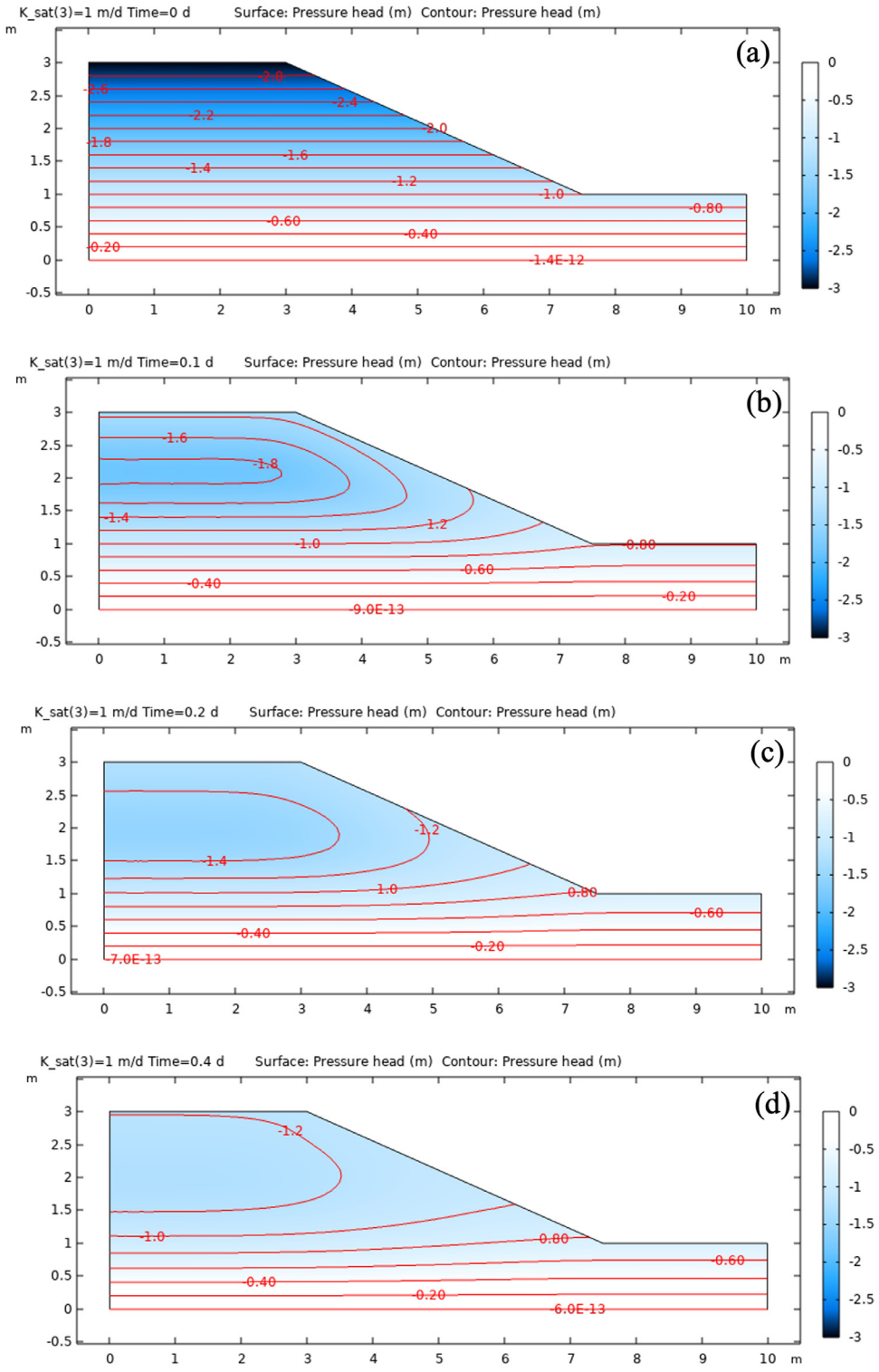

Fig. 5. Variation of pressure head after rainfall: (a) $t=0$; (b) $t=0.1$ *d*; (c) $t=0.2$ *d*; (d) $t=0.4$ *d*

matric suction head (negative pressure head) decreases with the depth and it becomes zero at the water table ($x=0$ m) and the maximum is 3.0 m. Fig. 5b shows the pressure head in the slope at $t=0.1$ d The matric suction is dissipated after rainfall. The matric suction head is 1.4 m at the top of the slope. When the rainfall proceeds, the matric suction head keeps reducing constantly. At $t=0.2$ d, the matric suction head is around 1.4 m at the slope crest (Fig. 5c). It is reduced to around 1.2 m after 0.4 days of rainfall.

Fig. 6 shows the variation of stress and settlement of the unsaturated soil slope under rainfall and load. The slope deformation is magnified by a factor of 10 to make it easier to observe. Fig. 6a is the initial stress under gravity before loading. The stress and settlement are slight at the slope crest. After applying a load, the stress and settlement at the slope crest significantly increase and can be up to 60 kPa (Fig. 6b)., The stress at the slope crest is reduced to around 10 kPa when the rainfall begins (Fig. 6c) and it

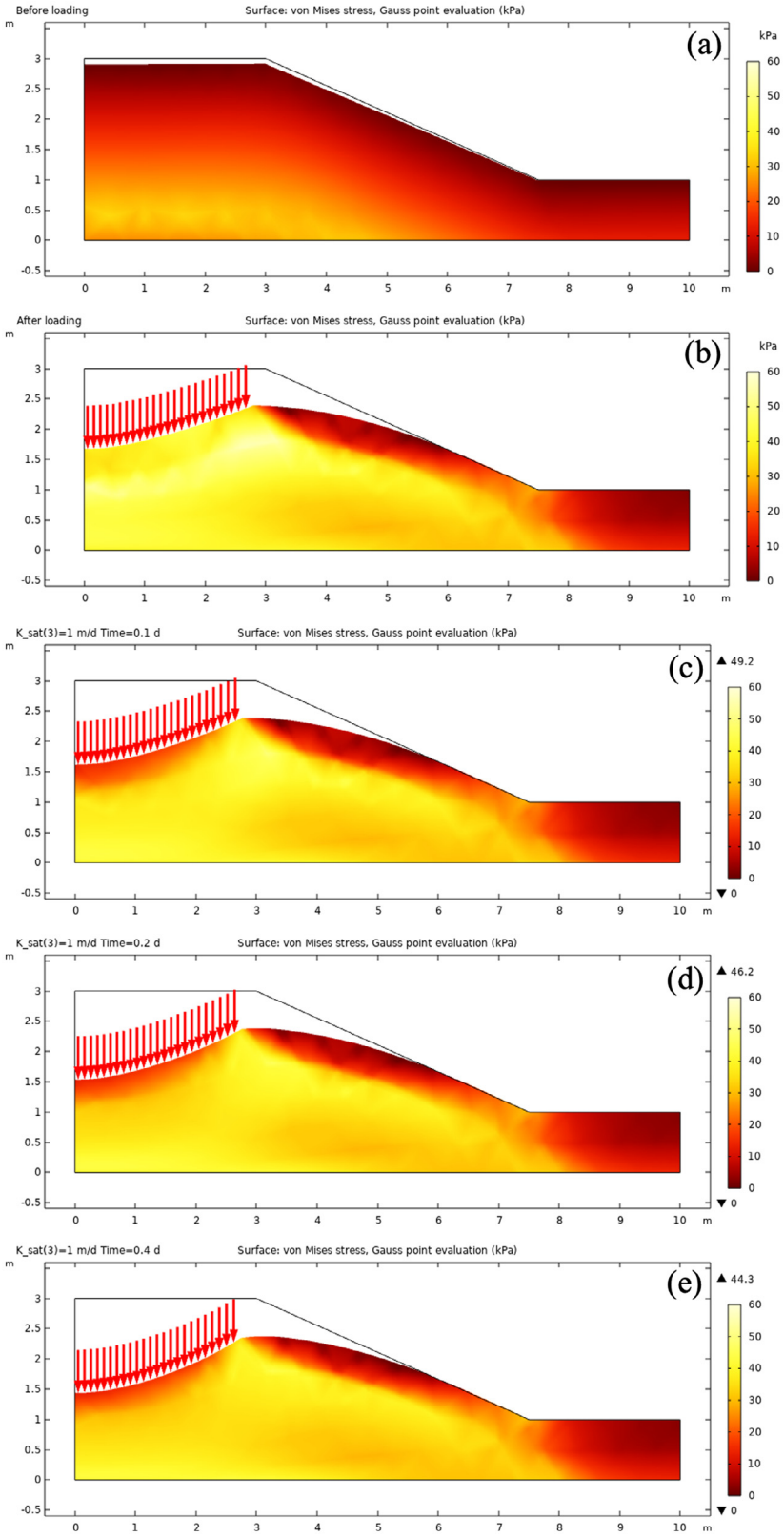

Fig. 6. Stress and settlement (Scale factor = 10): (a) Before loading; (b) After loading; (c) $t = 0.1\ d$; (d) $t = 0.2\ d$; (e) $t = 0.4\ d$

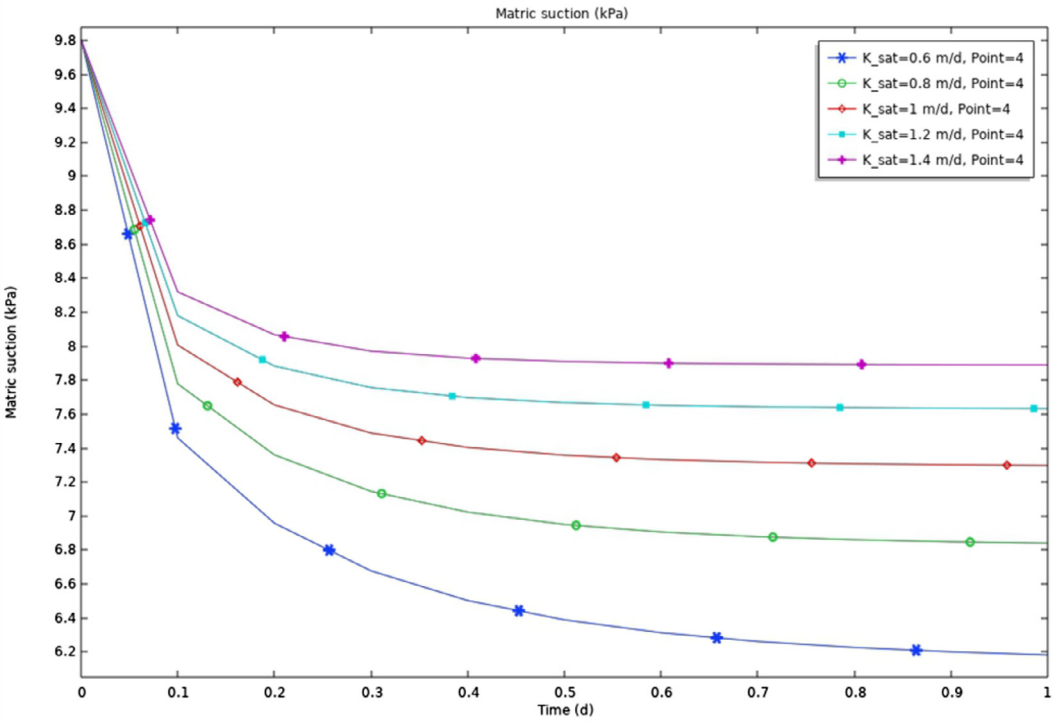

Fig. 7. Effect of saturated hydraulic conductivity on soil matric suction at slope toe.

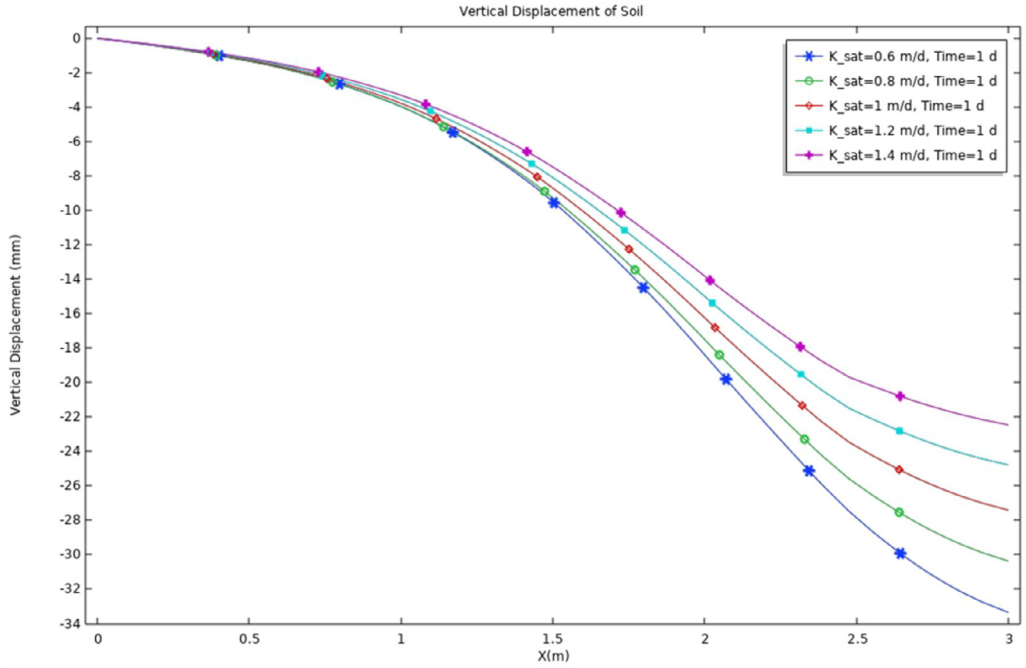

Fig. 8. Effect of saturated hydraulic conductivity on settlement at slope crest after 1-day rainfall.

continues to decline slightly as the rainfall progresses (Fig. 6d and e). However, the settlement is not significantly grown after rainfall. The settlement increases by about 4 cm after 0.4 days of rain.

Fig. 7 investigates the effect of saturated hydraulic conductivity k_s on soil matric suction at slope toe ($x = 7.5$ m, $z = 1$ m). The matric suction is reduced after rainfall. When the soil is assumed to be silty sand and $k_s = 1$ m/d is adopted, the matric suction is reduced from 9.8 kPa at the beginning and tends to be steady at 7.4 kPa. As k_s increases, the magnitude of the decrease in matric suction decreases. When $k_s = 0.6$ m/d (loess soil), the matric suction reduces by 1.8 kPa after rainfall, and it is 3.6 kPa for k_s =1.4 m/d (fine sand).

Fig. 8 displays the effect of saturated hydraulic conductivity on the settlement at the slope crest after 1-day rainfall. The abscissa represents the distance from the left boundary. The settlement increases with the distance. For a fixed location, the settlement decreases as k_s increases. Therefore, improving soil permeability is an effective way to control settlement.

Fig. 9 shows the effect of k_s on the pressure head profile at the slope crest ($x = 2$ m). The black line represents the initial condition

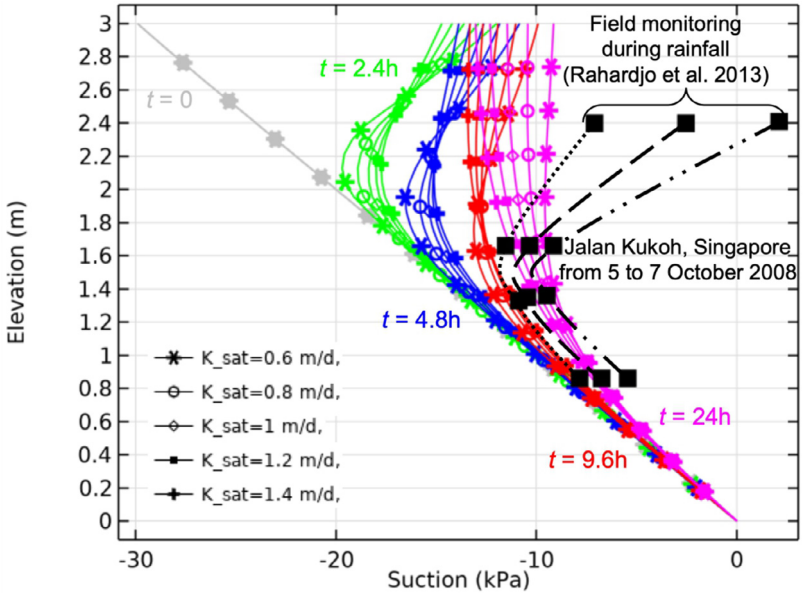

Fig. 9. Effect of saturated hydraulic conductivity on pressure head profile at slope crest ($x = 2$ m) and comparison to the field monitoring data at Jalan Kukoh, Singapore.

of hydrostatic. The wetting front is distinct at $t = 0.1$ d It goes down and vanishes as rainfall goes. When $t = 1$ d, the wetting front is no longer obvious and the pressure head profile is approximately to be steady state. The wetting front is more apparent as the k_s is reduced as the curvature of the pore pressure profile is more pronounced. The pressure head profile at a nearly steady state is also affected by the k_s. For example, when $k_s = 0.6$ m/d, the matric suction is at $t = 1$ d is around 0.9 kPa and it is 1.25 kPa for $k_s = 1.4$ m/d. The matric suction at a steady state is decreased when the k_s becomes small.

As mentioned above, soil suction plays an important role in rainfall-induced landslides, especially for small-scale slopes. Therefore, in this study, the simulated soil suction is compared to the field monitoring data in Singapore (Rahardjo et al., 2013). The slope is located in the residual soil from the sedimentary Jurong Formation at Jalan Kukoh. Several piezometers were installed on the slope to monitor soil suction. Fig. 9 also shows the soil suction in the middle of the slope from the piezometers. The wetting front is around 1 m below the surface during the rainfall event, which is similar to the simulated soil suction at $t = 9.6$ h. Generally, the simulated results are comparable to these field monitoring data, illustrating the justification of the hydro-mechanical model. However, the simulated wetting front is less sharp than the field monitoring. This may be because the hydraulic parameters used in this study are not strictly taken from Rahardjo et al. (2013) and evaporation is not considered.

4. Conclusions

In this study, a numerical model of a slope under rainfall and load is established by COMSOL Multiphysics. To facilitate the analysis for practical purposes, two built-in modules are used to model a unidirectional coupling of hydro-mechanical behaviors of unsaturated soil slopes. The Richards' module is first adopted to model an unsaturated soil slope under rainfall. Then the Extended Barcelona Basic module that considers the matric suction is adopted as the constitutive model. The effect of rainfall duration and saturated hydraulic conductivity on stress, settlement, and pore-water pressure are studied. The major conclusions are summarized below:

(1) When the rainfall proceeds, the matric suction head keeps reducing constantly. The settlement is not significantly grown after rainfall. The settlement increases by about 4 cm after 0.4 days of rain.
(2) When $k_s = 0.6$ m/d (loess soil), the matric suction reduces by 1.8 kPa after rainfall, and it is 3.6 kPa for $k_s = 1.4$ m/d (fine sand). For a fixed location, the settlement decreases as k_s increases. Therefore, improving soil permeability is an effective way to control settlement.
(3) The wetting front is more apparent as the k_s is reduced as the curvature of the pore pressure profile is more pronounced. The matric suction at a steady state is decreased when the k_s becomes small.

Declaration of interests

The authors declare that they have no known competing financial interests or personal relationships that could have appeared to influence the work reported in this paper.

References

Abed, A.A., Vermeer, P.A., 2009. Numerical simulation of unsaturated soil behaviour. Int. J. Comput. Appl. 34 (1), 2–12.
Alonso, E.E., Gens, A., Josa, A., 1990. A constitutive model for partially saturated soils. Géotechnique 40 (3), 405–430.
Borja, R.I., White, J.A., Liu, X., Wu, W., 2012. Factor of safety in a partially saturated slope inferred from hydro-mechanical continuum modeling. Int. J. Number. Anal. Methods Geomech. 36 (2), 236–248.
Casalbore, D., Passeri, F., Tommasi, P., Verrucci, L., Bosman, A., Romagnoli, C., Chiocci, F.L., 2020. Small-scale slope instability on the submarine flanks of insular volcanoes: the case-study of the Sciara del Fuoco slope (Stromboli). Int. J. Earth Sci. 109 (8), 2643–2658.
Crosta, G.B., Imposimato, S., Roddeman, D., Chiesa, S., Moia, F., 2005. Small fast-moving flow-like landslides in volcanic deposits: the 2001 Las Colinas Landslide (El Salvador). Eng. Geol. 79 (3–4), 185–214.
Cui, Y., Xu, C., Xu, S., Chai, S., Fu, G., Bao, P., 2020. Small-scale catastrophic landslides in loess areas of China: an example of the March 15, 2019, Zaoling landslide in Shanxi Province. Landslides 17 (3), 669–676.
Deng, S., Yang, H.Q., Chen, X., Wei, X., 2022. Probabilistic analysis of land subsidence due to pumping by Biot poroelasticity and random field theory. J. Eng. Appl. Sci. 69 (1), 1–18.
Farthing, M.W., Ogden, F.L., 2017. Numerical solution of Richards' equation: a review of advances and challenges. Soil Sci. Soc. Am. J. 81 (6), 1257–1269.
Kelner, M., Migeon, S., Tric, E., Couboulex, F., Dano, A., Lebourg, T., Taboada, A., 2016. Frequency and triggering of small-scale submarine landslides on decadal timescales: analysis of 4D bathymetric data from the continental slope offshore Nice (France). Mar. Geol. 379, 281–297.
Li, H., Zhang, L., Fredlund, D.G., Chen, L., Feng, S., Yang, H.Q., 2023. Hydraulic Responses of railway embankments using coupled moisture-heat flow modeling: effects of fill materials and climate conditions. Int. J. Civ. Eng. online.

Leong, E.C., Rahardjo, H., 1997. Review of soil-water characteristic curve equations. J. Geotech. Geoenviron. Eng. 123 (12), 1106–1117.
Liang, T., Knappett, J.A., Bengough, A.G., Ke, Y.X., 2017. Small-scale modelling of plant root systems using 3D printing, with applications to investigate the role of vegetation on earthquake-induced landslides. Landslides 14 (5), 1747–1765.
Navarro, V., Asensio, L., Alonso, J., Yustres, A., Pintado, X., 2014. Multiphysics implementation of advanced soil mechanics models. Comput. Geotech. 60, 20–28.
Ni, J.J., Leung, A.K., Ng, C.W.W., Shao, W., 2018. Modelling hydro-mechanical reinforcements of plants to slope stability. Comput. Geotech. 95, 99–109.
Olivares, L., Damiano, E., 2007. Postfailure mechanics of landslides: laboratory investigation of flow slides in pyroclastic soils. J. Geotech. Geoenviron. Eng. 133 (1), 51–62.
Pajalić, S., Peranić, J., Maksimović, S., Čeh, N., Jagodnik, V., Arbanas, Ž., 2021. Monitoring and data analysis in small-scale landslide physical model. Appl. Sci. 11 (11), 5040.
Pedroso, D.M., Farias, M.M., 2011. Extended Barcelona basic model for unsaturated soils under cyclic loadings. Comput. Geotech. 38 (5), 731–740.
Perzyna, P., 1966. Fundamental problems in viscoplasticity. Adv. Appl. Mech. 9, 243–377.
Pitts, J., 1984. A review of geology and engineering geology in Singapore. Q. J. Eng. Geol. Hydrogeol. 17 (2), 93–101.
Qi, S., Vanapalli, S.K., 2015. Hydro-mechanical coupling effect on surficial layer stability of unsaturated expansive soil slopes. Comput. Geotech. 70, 68–82.
Rahardjo, H., Leong, E.C., Gasmo, J.M., Tang, S.K., 1998. Assessment of rainfall effects on stability of residual soil slopes. In: Proceedings of the Second International Conference on Unsaturated Soils UNSAT, 98, pp. 78–83.
Rahardjo, H., Satyanaga, A., Leong, E.C., 2013. Effects of flux boundary conditions on pore-water pressure distribution in slope. Eng. Geol. 165, 133–142.
Richards, L.A., 1931. Capillary conduction of liquids through porous mediums. Physics (College Park Md) 1 (5), 318–333.
Satyanaga, A., Kim, Y., Hamdany, A.H., Nistor, M.M., Sham, A.W.L., Rahardjo, H. 2021. Preventive measures for rainfall-induced slope failures in Singapore. In Climate and Land Use Impacts on Natural and Artificial Systems. 205–223.
Sillers, W.S., Fredlund, D.G., 2001. Statistical assessment of soil-water characteristic curve models for geotechnical engineering. Can. Geotech. J. 38 (6), 1297–1313.
Tamagnini, R., 2004. An extended Cam-clay model for unsaturated soils with hydraulic hysteresis. Géotechnique 54 (3), 223–228.
Thanh, D.T., Long, N.T., 2019. Analysis the effects of the degree of saturation on the slopes stability using modelling and numerical simulation. Int. J. GEOMATE. 17 (63), 119–125.
Toll, D., 2001. Rainfall-induced landslides in Singapore. Proc. Inst. Civ. Eng.: Geotech. 149 (4), 211–216.
Wang, H., Sun, P., Wang, G., Wu, L., 2021. Experimental and numerical study of shallow loess slope failure induced by irrigation. Catena 206, 105548.
Wei, X., Zhang, L., Yang, H.Q., Zhang, L., Yao, Y.P., 2021. Machine learning for pore-water pressure time-series prediction: application of recurrent neural networks. Geosci. Front. 12 (1), 453–467.
Wood, D.M., 1990. Soil Behaviour and Critical State Soil Mechanics. Cambridge University Press.
Yang, H.Q., Yan, Y., Wei, X., Shen, Z., Chen, X., 2023. Probabilistic analysis of highly nonlinear models by adaptive sparse polynomial chaos: Transient infiltration in unsaturated soil. Int. J. Comput. Methods doi:10.1142/S0219876223500068.
Yang, H.Q., Zhang, L.L., Gao, L., Phoon, K.K., Wei, X., 2022. On the importance of landslide management: insights from a 32-year database of landslide consequences and rainfall in Hong Kong. Eng. Geol. 299, 106578.
Yang, H.Q., Zhang, L.L., Pan, Q., Phoon, K.K., Shen, Z., 2021. Bayesian estimation of spatially varying soil parameters with spatiotemporal monitoring data. Acta Geotech. 16 (1), 263–278.
Yang, H.Q., Chen, X., Zhang, L., Zhang, J., Wei, X., Tang, C., 2020. Conditions of hydraulic heterogeneity under which Bayesian estimation is more reliable. Water (Basel) 12 (1), 160.
Yang, K.H., Uzuoka, R., Lin, G.L., Nakai, Y., 2017. Coupled hydro-mechanical analysis of two unstable unsaturated slopes subject to rainfall infiltration. Eng. Geol. 216, 13–30.
Yeh, H.F., Tsai, Y.J., 2018. Analyzing the effect of soil hydraulic conductivity anisotropy on slope stability using a coupled hydromechanical framework. Water (Basel) 10 (7), 905.
Zhang, L.L., Fredlund, D.G., Fredlund, M.D., Wilson, G.W., 2014. Modeling the unsaturated soil zone in slope stability analysis. Can. Geotech. J. 51 (12), 1384–1398.
Zhang, L.L., Fredlund, D.G., Zhang, L.M., Tang, W.H., 2004. Numerical study of soil conditions under which matric suction can be maintained. Can. Geotech. J. 41 (4), 569–582.
Zhang, L.L., Wu, F., Zheng, Y., Chen, L., Zhang, J., Li, X., 2018. Probabilistic calibration of a coupled hydro-mechanical slope stability model with integration of multiple observations. Georisk 12 (3), 169–182.
Zhang, L.L., Wu, F., Wei, X., Yang, H.Q., Fu, S., Huang, J., Gao, L., 2022. Polynomial chaos surrogate and Bayesian learning for coupled hydro-mechanical behavior of soil slope. Rock Mech. Bull., 100023.
Zhang, L.L., Zhang, L.M., Tang, W.H., 2005. Rainfall-induced slope failure considering variability of soil properties. Geotechnique 55 (2), 183–188.
Zhang, L.L., Zhang, J., Zhang, L.M., Tang, W.H., 2011. Stability analysis of rainfall-induced slope failure: a review. Proc. Inst. Civ. Eng.: Geotech. 164 (5), 299–316.